Computational aspects of the smectization process in liquid crystals: An example study of a perfectly aligned two-dimensional hard-boomerang system

Agnieszka Chrzanowska*
Institute of Physics, Kraków University of Technology, ulica Podchorążych 1, 30-084 Kraków, Poland
(Received 24 February 2017; published 27 June 2017)

A replica method for calculation of smectic liquid crystal properties within the Onsager theory has been presented and applied to an exemplary case of two-dimensional perfectly aligned needlelike boomerangs. The method allows one to consider the complete influence of the interaction terms in contrast to the Fourier expansion method which uses mostly first or second order terms of expansion. The program based on the replica algorithm is able to calculate a single representative layer as an equivalent set of layers, depending on the size of the considered width of the sample integration interval. It predicts successfully smectic density distributions, energies, and layer thicknesses for different types of layer arrangement—of the antiferroelectric or of the smectic A order type. Specific features of the algorithm performance and influence of the numerical accuracy on the physical properties are presented. Future applications of the replica method to freely rotating molecules are discussed.

DOI: 10.1103/PhysRevE.95.063316

I. INTRODUCTION

Smectic liquid crystals are liquid crystals that exhibit, besides orientational order, also spatial regular modulation—they form layers. Within each layer particles can freely move like in a liquid, yet their orientational properties can exhibit different characteristics leading to different forms of smectics [1]. Most knowledge about smectic phases come from experimental evidence. From the theoretical point of view such phases are difficult to study due to the complicated spatio-orientational couplings.

There was always a strong interest to use theories like density functional theory (DFT) [2] or mean field (MF) theory to confirm or to predict physical properties of smectics. The earliest successful DFTs in liquid crystals assumed only one angle dependence and were able to provide solutions only for the uniaxial nematic phase [3]. A similar feature is exhibited in the MF model of Maier and Saupe [4]. With the increasing power of computers these approaches have been extended to find biaxial solutions, where the distribution functions depend on all three Euler angles [5,6]. One of the first attempts to provide a theory of smectics was the theory of McMillan [7]. It considered a description of the smectic phase by a mean field potential given in terms of the leading order parameters related to orientational order as well as to the density wave characteristics. Formally, it was an extension of the Maier-Saupe model of the nematic phase to the case of the smectic A phase. Marguta *et al.* [8] extended the McMillan model to the case that uses an infinite set of the orientational and translational order parameters and showed to what extent the McMillan model underestimates both orientational and translational order and the transition entropies. The importance of using higher harmonics in the Fourier expansion was also discussed by Longa in the context of the location of the tricritical nematic-smectic A point [9]. Throughout the following years a great number of published reports showed that the mean field approach can be also successfully applied for the description of other more complicated types of smectics (for instance, [10–18]).

It is a more challenging task to obtain full dependence of the distribution functions on the spatial as well as on the orientational variables for a given intermolecular potential. For this purpose different types of density functional theories are in use and the knowledge is still accumulating [19–24]. From the computational point of view all of them resort to solving integral equations or to minimizing the free energy functional, which also contains multidimensional integrals.

One way to avoid tedious numerical integration is to assume in advance the type of solution, for instance the already mentioned above series of the Fourier functions, and then to find iteratively appropriate expansion parameters. Such a procedure will be restricted, however, to the number of terms in the considered formulas. Due to Velasco *et al.* [23] or, also, Martínez-Ratón and Velasco [24], an alternative way is to find a single characteristic function that would mimic the shape of the smectic density profile. For a smectic layer profile an exponent $\exp(\lambda \cos(qy))$ has been used. This choice, however relatively simple to use in calculations, would not be suitable for incommensurate phases or for the phases in which the distributions are not symmetric functions.

The question can be posed whether it would be possible to find a full solution without expanding distribution functions in the series of the symmetry adapted functions or without imposing mathematical restriction on the outcome. Surprisingly, such a problem was easier to solve in the case of confined liquid crystals than in the case of bulk smectics. In [25] a method of finding spatially irregular orientational solutions for a liquid crystal placed in a slab geometry between two walls has been described. This method, which was based on the Gaussian quadratures application, has been successfully used to study inhomogeneous confined thin films of liquid crystals like a fluid of hard Gaussian overlap particles [26–29] or the Gay-Berne particles model [30].

The benefit of the Gaussian integration method lies in the fact that it uses a small number of integration points and is very quick. In the geometry used in [25] it was feasible to use this methods for spatial integration since the integral limits were the same as the scope of the distribution function dependence.

*achrzano@usk.pk.edu.pl

In the case of bulk systems this is no longer valid—one cannot obtain solutions described on the infinite spatial interval unless the considered systems are uniform or periodic.

Periodic spatial structures, like smectics in liquid crystals, are bulk systems. Since their characteristics repeat regularly in space in reality the needed spatial dependence can be limited to a certain interval. A question is how to find such an interval that would be commensurate with the true structure periodicity. This is not just a problem about the smectic layer thickness that minimizes the free energy; the main problem (see below) lies in the fact that while solving the self-consistency equations for the spatially dependent distributions one deals with an *infinite spatial integral*.

In what follows we present a natural and simple numerical algorithm together with the results of its application to the smectic formation problem. As is always important in computational physics, the main aspect is also how the numerical accuracy of undertaken procedures influences the reliability of the predicted physical properties.

This paper is organized as follows. Section II provides the basis of the Onsager theory adjusted to the smectic geometry for the case of a two-dimensional smectic liquid crystal with a simplifying assumption of perfect alignment. Section III gives the details of the used numerical scheme and Sec. IV provides the numerical solutions together with the discussion of the influence of the numerical accuracy on the obtained physical properties. Section V is the summary.

II. ONSAGER THEORY

Let us consider a system composed of N particles whose state is given by the spatio-orientational distribution function ρ. The function ρ is the probability to find a particle at the point $\mathbf{r}$ and having the orientation Ω. It is normalized to the number of particles, N:

$$\int \rho \, d\mathbf{r} \, d\Omega = N. \tag{1}$$

The Helmholtz free energy of the system made of different types of particles described by the indices i and j is given by the formula

$$\beta F = \sum_i \int \rho_i (\ln \rho_i - 1) \, d(i) - \frac{1}{2} \sum_{i,j} \int (e^{-\beta U_{ij}} - 1) \rho_i \rho_j \, d(i) \, d(j), \tag{2}$$

where index i or j denotes the type of the particle. As the type of the particle we also understand a different conformation. In (2) $d(i) \equiv d\mathbf{r}_i \, d\Omega_i$; β is $\beta = 1/kT$, where k is the Boltzmann constant and T is the temperature; U_{ij} is the interparticle potential acting between molecules i and j; and $(e^{-\beta U_{ij}} - 1)$ is the so-called Maier function.

The minimum condition for particle type i reads

$$\frac{\delta(\beta F)}{\delta \rho_i} = 0, \tag{3}$$

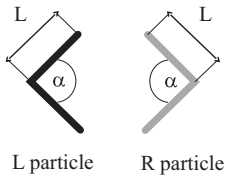

FIG. 1. Boomerang particles. The arm length is given by L and the apex angle is α. Boomerangs are perfectly aligned and two orientations are considered, R and L. Different shading is used to distinguish particles with different orientation.

which leads to the self-consistency (Onsager) equations of the form

$$\ln \rho_i = \sum_j \int (e^{-\beta U_{ij}} - 1) \rho_j \, d(j). \tag{4}$$

Solutions of these equations depend on the type of the interacting particles and assumed interactions U_{ij}.

In this work we consider particles in the form of needlelike boomerangs as in Fig. 1 that are characterized by the length of the arm, L, and the apex angle α. The boomerangs are perfectly aligned, yet they can attain two orientations. (For the bifurcation analysis and phase diagram for such a system one can see in [31].) Boomerangs pointed to the right are denoted by the index R and boomerangs pointed to the left by the index L.

For this case Eq. (4) takes the form

$$\ln \rho_R = \int (e^{-\beta U_{RR}} - 1) \rho_R \, d(R) + \int (e^{-\beta U_{RL}} - 1) \rho_L \, d(L),$$
$$\ln \rho_L = \int (e^{-\beta U_{LL}} - 1) \rho_L \, d(L) + \int (e^{-\beta U_{RL}} - 1) \rho_R \, d(R). \tag{5}$$

For rigid bodies and the possibility of spatially modulated solutions the Maier function can be integrated over the variable perpendicular to the assumed axis of modulation, which in the two-dimensional (2D) case leads to the transformation of the Maier function to the form of the excluded area S^{excl}. Since intermolecular potential U_{ij} is zero, when particles are apart, and infinite if they overlap, then the Maier function $(e^{-\beta U_{ij}} - 1)$ is zero when they are apart and -1 when they overlap. Hence the integral

$$-\int (e^{-\beta U_{ij}} - 1) \, dx_{ij} = S^{\text{excl}}(y_{ij}) \tag{6}$$

becomes $S^{\text{excl}}(y_{ij})$. How to calculate $S^{\text{excl}}(y_{ij})$ is explained in the next section.

Because the modulation axis has been chosen as the Y axis, the distribution functions depend only on the y variable. If one knows beforehand the period of modulations, the problem would be very easy: it would be sufficient to provide the solutions only for this scope. But the period of the solutions is unknown. Another difficult problem is also that the integrals in Eq. (4) are infinite.

To solve the Onsager equations the following scheme has been proposed.

III. DESCRIPTION OF THE SOLVING SCHEME

A. Equations to be solved

Let us consider an interval along the Y axis of length S_d, which would correspond to the modulation period or a multiple of this period. The distribution ρ should be replaced now by its normalized to unity counterpart f defined as

$$\frac{1}{S_d}\int_{-S_d/2}^{S_d/2} f\,dy = 1, \tag{7}$$

which is the probability per unit length. In this formulation we have also assumed that the layer of width S_d contains N particles. The correspondence between f and ρ is

$$\rho = Cf, \tag{8}$$

where C is the proportionality constant.

To find out the proportionality constant C we put the above formula in the normalization condition (1) with respect to one type of particle, for instance, i. If perfect alignment is assumed and the particle's orientation is chosen (R or L) then there is no integration over the angles involved. Hence

$$\int C_i f_i\,dx\,dy = N_i, \tag{9}$$

where N_i is the number of particles i and C_i refers also to the particles of type i. Since there is no modulation of f_i in the X direction, the integration over the x variable gives the value of the integration interval S_x. Equation (9) can be rewritten now as

$$C_i S_x S_d \frac{1}{S_d}\int f_i\,dy = N_i \tag{10}$$

or

$$\frac{1}{S_d}\int f_i\,dy = \frac{N_i}{C_i S_x S_d}. \tag{11}$$

Using condition (7) in Eq. (11), it emerges that $C_i = d_i$, where $d_i = N_i/S$ is the surface density of particles i with $S = S_x S_d$.

The method of normalization is very important since upon this condition it depends whether we consider a mixture with fixed proportions of the components or a system with the spontaneous possibility to attain orientation R or L. If one assumes in Eq. (9) that the number of particles, N_i, is fixed, then the considered case will be a mixture (like in [32,33]). In this work, however, we focus on another case, i.e., when the particles can spontaneously change their orientations. In this case the normalization follows:

$$\frac{1}{S_d}\int (f_R + f_L)\,dy = 1 \tag{12}$$

and the density $d = N/S$ corresponds to all the particles in the system.

In terms of the functions f_R and f_L the self-consistency equations to be solved read

$$\begin{aligned}
\ln f_R &= -dx_R\int_{-\infty}^{+\infty} S_{RR}^{\text{excl}} f_R\,dy_R - dx_L\int_{-\infty}^{+\infty} S_{RL}^{\text{excl}} f_L\,dy_L\\
\ln f_L &= -dx_L\int_{-\infty}^{+\infty} S_{LL}^{\text{excl}} f_L\,dy_L - dx_R\int_{-\infty}^{+\infty} S_{LR}^{\text{excl}} f_R\,dy_R
\end{aligned} \tag{13}$$

where x_R and x_L are the fractions of the particles R and L. If one assumes that $x_R = 1$ and $x_L = 1$ and assumes the normalization condition as in Eq. (12) then Eqs. (13) will describe the system in which the amount of each type of particles is adjusted spontaneously according to the free energy minimum condition. This case is used in the analysis presented in this paper.

The integral equations (13) are the core of the Onsager theory. Not only do they contain infinite integrals but they also depend on the unknown interval S_d. Two questions occur now: how to solve them and how to find the optimal value of S_d.

The answer to the second question is straightforward. Provided that solutions are known for arbitrary values of S_d, the minimum of the Onsager free energy will provide a criterion for the required optimal S_d. In terms of f_R and f_L the free energy of the layer of the thickness S_d per particle can be calculated from Eq. (2) as

$$\begin{aligned}
\frac{\beta F}{N} &= [\ln(d) - 1] + \frac{1}{S_d}\sum_i \int_{-S_d/2}^{+S_d/2} f_i \ln(f_i)\,dy_i\\
&\quad + d\frac{1}{2S_d}\sum_{i,j}\int_{-S_d/2}^{+S_d/2} dy_i \int_{-\infty}^{+\infty} S_{ij}^{\text{excl}} f_i f_j\,dy_j,
\end{aligned} \tag{14}$$

where $i,j = R,L$. This formula also contains an infinite integral.

The most important problem is how to solve Onsager equations (13) for an arbitrary value of S_d and how to obtain the appropriate free energy if they contain infinite integrals.

A typical way of solving Eqs. (13) is to evaluate integrals on the right hand side of Eqs. (13) by the use of arbitrarily chosen starting values of f_R and f_L, obtaining new estimates for these distributions, and then calculating again the above integrals. Such a procedure should be repeated iteratively until the new values of f_R and f_L agree with the values from the previous iteration step. In the case of periodic solutions that span over the infinite regime the most difficulty lies in the integration scheme.

B. Establishing lattice and nodes for the integration scheme

All integration methods are based on the values of the functions calculated at the chosen nodes of the integral interval. In what follows we use the simplest of them—the trapezoidal method—since in this case making replicas (to be explained further) is the quickest. Note, however, that the replica method can be adapted in any integration scheme.

In order to establish the lattice of nodes for the integration scheme let us consider an interval in the Y-axis direction of length S_d (we call it the central box) and two adjacent intervals of the same length, within which we later place replicas of the solutions from the interval S_d (like in Fig. 2). At the initial stage there is no notion of how large such an interval should be. The only information is the fact that it probably should be commensurate with the interaction regime, which in the case of the hard-body interactions will correspond to the size of the particles. In practice, we start with the values slightly larger than the projection of the boomerangs on the Y axis.

The central box and two adjacent boxes altogether cover the $3S_d$ distance. Within this integration interval we place N_n

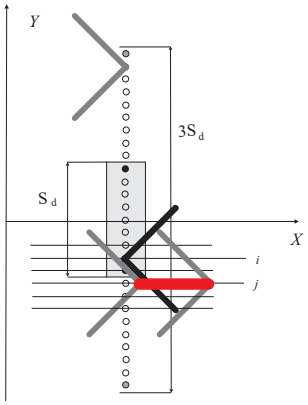

FIG. 2. Geometry of the integration points along the Y axis. The size of S_d should be such that the particles placed at the outermost points from the central interval and from the neighboring interval will not lead to an overlap while the particles are being moved along the X axis; i.e., their excluded X interval for such points is already zero. An example of the excluded slice for the boomerangs at y_i and y_j is given as a thick solid (red) line.

nodes so that they are in equispaced positions. The number of nodes, N_n, can be assumed as needed. In Fig. 2 these nodes are given as circles. Each node j is determined by the value of its coordinate y_j. To calculate integrals on the right hand side of Eqs. (13) we need values of distributions $f_R(y_j)$ and $f_L(y_j)$ at the nodes y_j and also the values of the interaction kernel, here $S^{\text{excl}}(y_i, y_j)$. Within the process of the iteration the distributions (their estimates) $f_R(y_j)$ and $f_L(y_j)$ will change their values, but interaction kernel will be always the same. This means that one can calculate values of $S^{\text{excl}}(y_i, y_j)$ at the beginning of the iteration scheme and tabulate them for later use at each step of the iteration.

C. Replica method of solving self-consistency equations

The replica idea applied to the Onsager equations concerns the usage of the set of nodes. The distribution functions needed on the right hand side of Eqs. (13) are to be evaluated on the whole $3S_d$ interval, but the interaction kernel, $S^{\text{excl}}(i, j)$, in our method is treated differently: with respect to the second variable, y_j, it depends also on $3S_d$ intervals, yet with respect to the first variable, y_i, it depends only on the nodes from the central box. Such a notation that the index i refers only to the nodes from the central box and the index j will cover nodes from the central and from the adjacent boxes is also further used.

The first evaluation means that we take starting (any) values of $f_R(y_j)$ and $f_L(y_j)$ for the whole $3S_d$ interval and we take values of $S^{\text{excl}}(y_i, y_j)$ for the interval, where y_j is also for the whole $3S_d$ interval but y_i is only for the central box, and we calculate new estimates of $f_R(y_i)$ and $f_L(y_i)$ (in fact, logarithms of them).

The new estimates depend on the y_i variable from the central box, but for further use we need $f_R(y_j)$ and $f_L(y_j)$ for the large interval $3S_d$. The idea of replicas is just to use values from the central box and assume that the same outcome will exactly occur in the neighboring boxes. Numerically making replicas is just copying values of f_R and f_L for the nodes in the neighboring boxes. Once we have estimates of the distribution functions on the whole $3S_d$ interval we can use them for the next step of the iteration process.

D. On the calculation of $S^{\text{excl}}(y_i, y_j)$

For the purpose of the above scheme we must calculate values of $S^{\text{excl}}(y_i, y_j)$ at each pair y_i, y_j and store these values in a matrix form dependent on the indices i and j. By definition the excluded area is the area which is inaccessible to the center of the particle j while it is being moved around the particle i. This area is constructed from the intervals inaccessible to the particle j while it is being moved along the X axis in the presence of particle i with its position fixed at (x_i, y_i). It should be calculated for each pair of points i and j or, more precisely, for the variable $y_{ij} = y_i - y_j$.

We present how to calculate $S^{\text{excl}}(y_i, y_j)$ for the boomerangs from Fig. 1 in Fig. 2. As the first step we consider a boomerang i and place it at the node i from the central box in such a way that the apex point (instead of the geometrical center) is at $x_i = 0$ and $y_j = 0$. In Fig. 2 this boomerang is black. Then we take another boomerang j and place it in such a way that its apex point is at the level y_j. In Fig. 2 there are shown two such positions (the boomerangs are gray). The gray boomerang in the upper position, while being moved along the X axis, does not touch the black boomerang, since it is too high; hence $S^{\text{excl}}(y_i, y_j)$ is zero. For the gray boomerang at the lower level, while it is being moved along the X axis, one finds two distinct points of contact between the particles i and j. The distance between these points gives the value of $S^{\text{excl}}(y_i, y_j)$. In Fig. 2 this is depicted by a thick (red) interval.

Now one can also see how large the interval S_d should be. If we place the particle i at the outermost points from the central box and the particle j at the outermost nodes from the interval $3S_d$ and the resulting $S^{\text{excl}}(y_i, y_j)$ is zero, then one can assume that the size of S_d is sufficiently large. It can be of course larger, but the problem arises only when it is too small.

Once we know that two particles are so far away that there is no interaction between them there is no longer any contribution to the integral on the right hand side of Eqs. (13): all possible contributions have been already considered and initially infinite integrals become practically finite.

If all possible results for $S^{\text{excl}}(y_i, y_j)$ are calculated and put on a 2D diagram one obtains the full 2D excluded area. An example of such excluded areas for two needlelike boomerangs with infinitely thin arms from Fig. 1 are presented in Fig. 3. The shaded area together with the black border lines is the area which is inaccessible for the coordinates of the apex point of the boomerang j and represents the resultant excluded area. For two boomerangs with the same orientation the excluded area is given at the left hand side of Fig. 3 and it is exactly the same for the boomerangs pointed to the left or to the right. If the orientations of the particles are opposite, the shape of the excluded area, given on the right hand side of Fig. 3, is completely different. As it can be seen, in both cases these areas are defined by a set of straight lines. Their positions correspond to the shape of the particles. The conditions for the algebraic expressions that describe all these lines (parameters A and B for $y = Ax + B$ for each line) can be read out from the picture and put in the program for automatic calculation of $S^{\text{excl}}(y_i, y_j)$ for any points y_i and y_j.

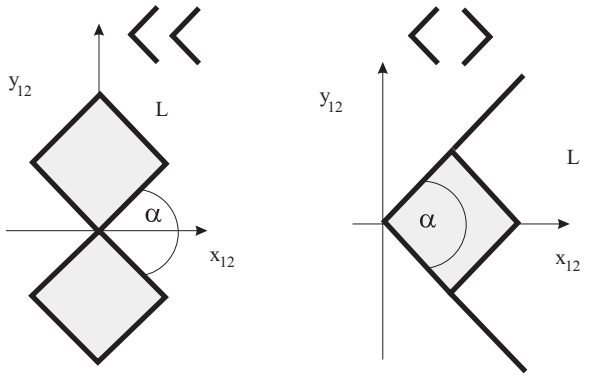

FIG. 3. Shape of the excluded areas for two different mutual orientations of boomerangs.

E. Iteration process details

To start the iteration process, besides the model parameters L, α, and S_d and emerging from them values of S^{excl}, one also needs the value of the density d and, as already mentioned, an initial set of values for f_L and f_R. As starting distributions we use the simplest periodical functions, i.e., the functions sine and cosine:

$$f_R = \cos\left(\frac{2\pi y}{A_R S_d}\right), \qquad f_L = \sin\left(\frac{2\pi y}{A_L S_d}\right), \tag{15}$$

with A_R and A_L being certain numbers allowing for a change of the periodicity of the initial conditions. They can be chosen arbitrarily. There is no need to normalize initial functions at the beginning, since normalization of the functions must be performed always at each step of the iteration process.

In general, Eqs. (13) can have many solutions of different kinds and the chance to find them will depend on the values of A_R and A_L. It would be good then to check as many sets of A_R and A_L as possible to see what types of solutions are being obtained. Once we know what functions are to be used as initial data we calculate the distribution functions [$f_R(y_j)$ and $f_L(y_j)$] at all nodes, from the central box as well as from the adjacent boxes, and store the outcome in a vector for further use. Performing integrals is just a summation of the appropriate values that are also stored in vectors or matrices. The new estimates of $f_R(y_i)$ and $f_L(y_i)$ are used as replicas to construct distributions over the entire $3S_d$ interval. The updated outcome should be next consistently used on the right hand side of Eqs. (13). Such an iteration procedure self-consistently is repeated until the following condition is fulfilled:

$$\text{error} < \epsilon, \tag{16}$$

where

$$\text{error} = \sum_i \left(\left|f_R^{\text{new}}(i) - f_R^{\text{old}}(i)\right| + \left|f_L^{\text{new}}(i) - f_L^{\text{old}}(i)\right|\right), \tag{17}$$

ϵ is the assumed accuracy number, and i is the index of the node. Labels in the superscript index, "new" and "old," refer to two subsequent values of distribution functions within the iteration process. To ensure convergence of the iteration procedure, in practice one needs also to use a mixture of the new and old solutions. Usually it works for a mixture of 90% of the old solution and 10% of the new one.

On the face of it such a replica method can give the impression of being wrong since surely there will be discontinuities at the border of the boxes, at least after the first iterations, as expected. But let us see how such an iteration scheme works.

IV. RESULTS

In this section the results of the Onsager theory are presented for different values of the theory parameters.

For the density corresponding to the smectic phase, $d = 200$, and parameters $\alpha = \pi/2$, $L = 0.1$, and $S_d = 0.16$ with the initial function parameters as $A_R = 1$ and $A_L = 1$ [see Eqs. (15)], the program converges to a solution like in Fig. 4(d). In Fig. 4 we also present intermediate stages of the iteration process: Fig. 4(a) shows the starting profiles of f_L and f_R according to Eqs. (15), Fig. 4(b) presents an intermediate stage of f_L and f_R when error $\leqslant \epsilon = 50$, Fig. 4(c) presents

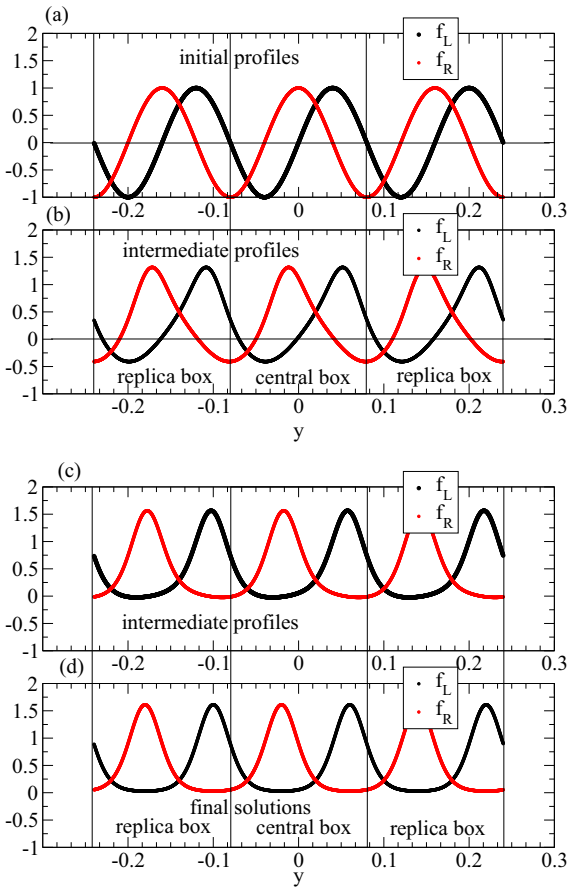

FIG. 4. Solutions f_L and f_R obtained from the initial configurations due to Eqs. (15) with $A_L = 1$ and $A_R = 1$: (a) starting profiles of f_L and f_R according to Eqs. (15); (b) an intermediate stage of f_L and f_R, when the error is error $\leqslant \epsilon = 50$; (c) an intermediate stage of f_L and f_R, when the error is error $\leqslant \epsilon = 10$; and (d) the final solutions of f_L and f_R, when the error is error $\leqslant \epsilon = 0.00001$. At each stage the solutions are continuous.

FIG. 5. Antiferroelectric phase.

an intermediate stage of f_L and f_R when error $\leqslant \epsilon = 10$, and Fig. 4(d) shows the final solutions of f_L and f_R for error $\leqslant \epsilon = 0.00001$.

Looking at these results the first observation is that all profiles obtained at different stages of iteration are continuous. The negative parts, which are present in the starting profiles, pertain for a number of initial iterations because of the fact that mixtures of old and new solutions are used. They eventually disappear: the whole profiles are gradually shifted up within the iteration process. At the same time the peaks are moved to the left or to the right and finally they find themselves in the regular intervals, which is characteristic for the regular layered formation.

The obtained final solutions are of the antiferroelectric type. In this type of order subsequent layers, whose positions are given by subsequent peaks, are of different orientations. The layer rich in the R boomerangs, whose center is given by the peak of the f_R function, is followed by a layer rich with the L boomerangs, whose center is given by the peaks of the f_L function. An artistic view of an antiferroelectric phase is given in Fig. 5.

So the first aim has been achieved: the replica method indeed leads to the physical solution of the modulated phases even for arbitrary S_d. In Fig. 4 one observes exactly three periods spanning the interval of the size of the central box and two adjacent replicas. Finding solutions for different values of S_d and checking corresponding values of the free energy due to Eq. (14), one can obtain an optimal value of the modulation structure period.

It turns out, however, that the condition of continuous initial functions does not mean that the intermediate profiles are always continuous, as feared at the beginning. The case shown in Fig. 6 gives an example when the initial condition, due to Eqs. (15) with $A_L = 0.4$ and $A_R = 0.7$, is continuous, yet, because of the S_d being incommensurate with these initial periods, it becomes immediately discontinuous. During the iteration process these discontinuities change their character and finally f_L and f_R attain the stage when they are continuous. In fact, the same solutions are being obtained as in Fig. 4, although they are slightly shifted in phase: the peaked profiles are the same, yet their positions are changed (moved). This

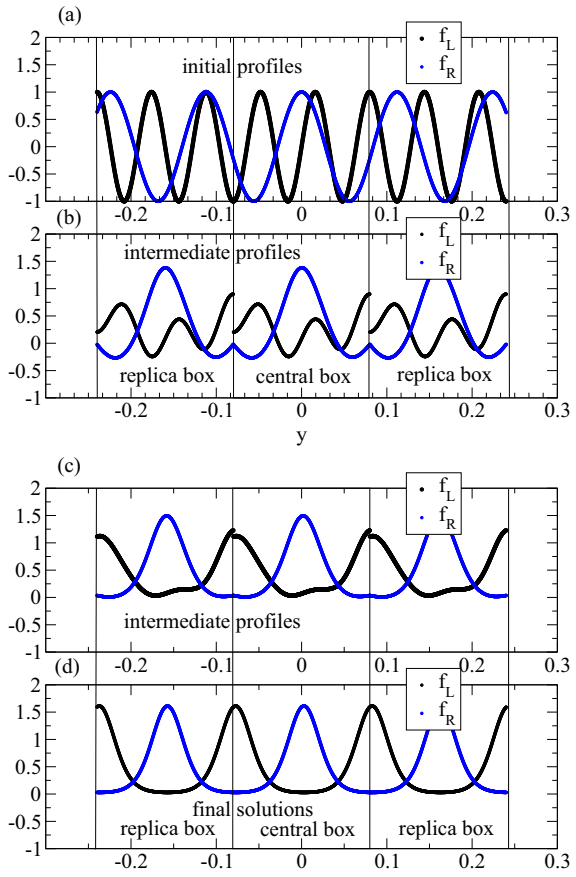

FIG. 6. Solutions f_L and f_R obtained from the initial configurations due to Eqs. (15) with $A_L = 0.4$ and $A_R = 0.7$: (a) starting profiles of f_L and f_R according to Eqs. (15); (b) an intermediate stage of f_L and f_R, when the error is error $\leqslant \epsilon = 50$; (c) an intermediate stage of f_L and f_R, when the error is error $\leqslant \epsilon = 10$; and (d) the final solutions of f_L and f_R, when the error is error $\leqslant \epsilon = 0.00001$. Periodicity of the initial profiles is much different from the final solutions which results in the fact that intermediate profiles are discontinuous, yet final solutions are continuous again.

change of the position of the peaks is very important as far as calculation of the order parameters is concerned.

The order parameters are needed in order to assess the degree of smectization of the system. They should provide universal information. To find them it is important to know how many layers are found within the main interval S_d. This number m should be included in the defining formulas for the order parameters S_R and S_L, which describe the strength of order of the boomerangs R and L, respectively:

$$S_L = \int_{-S_d/2}^{S_d/2} f_L(y) \cos\left(\frac{2\pi m y}{S_d}\right) dy,$$
$$S_R = \int_{-S_d/2}^{S_d/2} f_R(y) \cos\left(\frac{2\pi m y}{S_d}\right) dy. \tag{18}$$

In practice S_L and S_R will depend on the fact whether the profiles f_L and f_R are symmetric about the point $y = 0$. In order to have universal values we have to impose a condition that one of them, say f_R, has a maximum exactly at $y = 0$ and we have only one smectic layer within the interval S_d.

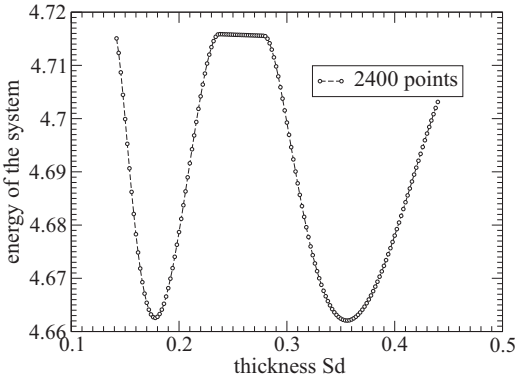

FIG. 7. Free energy versus S_d interval. Two subsequent minimums correspond to the same type of solution. The second minimum corresponds to the solutions covering twice the number of smectic layers as in the first minimum case.

Under this condition we can treat the outcome of Eqs. (18) as a good measure of the smectization degree. For the boomerang case given in Fig. 6 these values are $S_L = -0.3449$ and $S_R = 0.3449$. They have the same absolute value but opposite signs; such a feature is symptomatic of the order of the antiferroelectric type.

As already mentioned, the distance between two subsequent peaks, the layer thickness, is determined by the assumed number for S_d. This should be optimized. In order to obtain a realistic value of the layer thickness one needs now to scan over different values of the S_d parameter, calculate solutions of the self-consistency equations, and then find values of the free energy according to Eq. (14).

To analyze the free energy properties, in Fig. 7 the free energy profile versus the integration layer thickness has been given for the needlelike boomerangs of the apex angle $\alpha = \pi/2$, the arm length $L = 0.1$, and the system density $d = 170$. One observes here two minimums of the same depth. The first minimum occurs at the integration interval $S_d = 0.1775$ and the second minimum at $S_d = 0.355$. These two minimums, in fact, correspond to the same solution. In the case $S_d = 0.355$ the number of smectic layers is twice the number of smectic layers obtained for $S_d = 0.1775$. To see this in Fig. 8 we show that the free energy characteristics of two subsequent

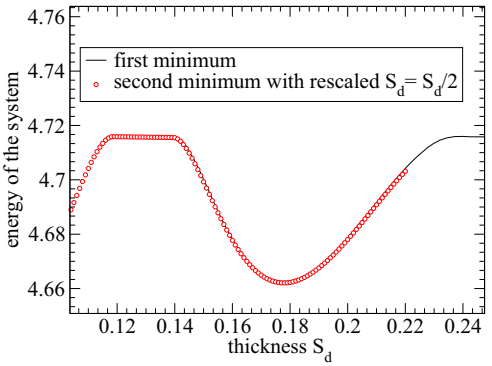

FIG. 8. Free energy versus S_d interval. Two subsequent minimums correspond to the same type of solution.

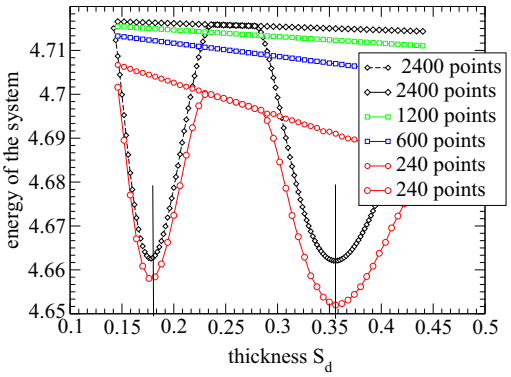

FIG. 9. Accuracy of free energy calculations with respect to the number of integration points.

minimums are, in fact, the same. If we divide S_d by 2 then we see that we obtain the second minimum in the place of the first minimum and exactly the same shape.

The minimums in Fig. 7 are of the same depth. Such results have been obtained for 2400 points that have been used in the assessment of the integrals. It is interesting now to see what will happen—if the number of integration points is smaller. In Fig. 9 we show a sequence of the free energy results obtained for different numbers of integration points. For the solutions without modulations the free energy should be at a constant level. Yet, due to the numerical inaccuracy, it has a diminishing tendency: it is stronger as a smaller number of integration points are used. For comparison purposes, an anisotropic solution is also presented for only 240 nodes. Now the second minimum is a bit deeper, yet its position is the same as in the previous case. If the numerical purpose is only to find the position of the minimum then the accuracy of computation and the number of integration points seems to be unimportant.

To see also that the second minimum corresponds to the case with a doubled number of layers, let us also have a look at the distribution functions obtained for the above two values of the integration interval. They are presented in Fig. 10. The solutions f_L and f_R for $S_d = 0.1775$ exhibit only three peaks. For $S_d = 0.355$, f_L and f_R exhibit six peaks: twice as many as in the former case. The peaks are of the same height, which

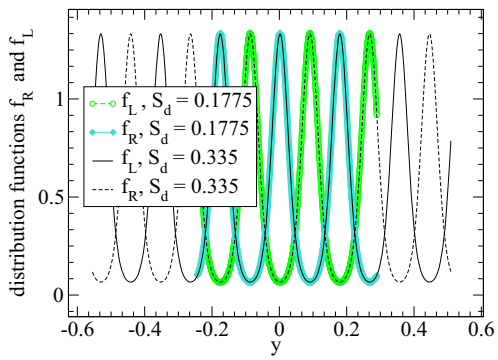

FIG. 10. The distribution profiles f_R and f_L for $S_d = 0.1775$ and $S_d = 0.335$. These are the same functions, but for a longer interval of S_d the number of smectic layers obtained is twice the number as in the case of $S_d = 0.1775$.

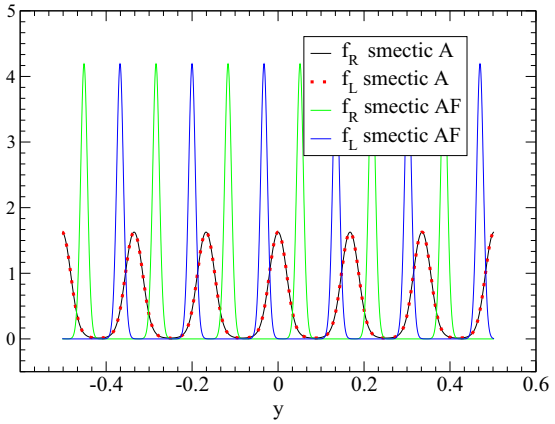

FIG. 11. Comparison of the distributions for the smectic A case and for the antiferroelectric smectic obtained for the same density, $d = 800$. In the smectic A case the free energy is $E = 10.76$ and in the AF smectic it is $E = 7.317$.

emerges from the fact of the normalizing condition (7), which contains the term $1/S_d$.

Besides the antiferroelectric order, for hard boomerangs it is also possible to obtain another solution. If the density comes from the region beyond the bifurcation point from the uniaxial phase to the smectic A phase, one can obtain f_L and f_R which describe the smectic A type.

An example of such a solution is given in Fig. 11. In the case of the smectic A phase, the distribution functions f_R and f_L are the same and the layer width is twice the layer width of the antiferroelectric (AF) case. In contrast, the solutions for the AF order exhibit steep peaks, which correspond to well ordered layers. The layers composed of the R particles are practically free of the L particles. Contrarily, the peaks of the smectic A phase are much smaller and softer. One also observes here larger areas which are completely free of all types of particles. Comparing energies one sees that the antiferroelectric phase is more stable than the smectic A phase. An artistic view of the smectic A phase is given in Fig. 12.

No polar smectic phase has been encountered for the needlelike boomerangs.

It would be interesting now to compare the outcome of the present calculations with the most successful fitting function for the smectic density profiles. It has been considered, for

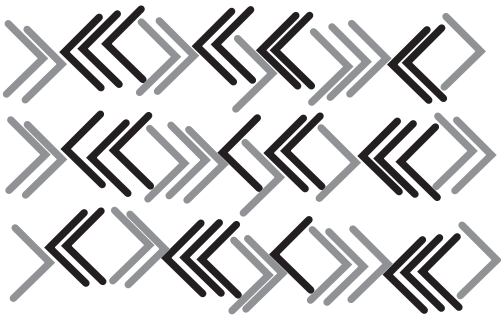

FIG. 12. Smectic A occurs when the numbers of left and right particles within each layer are on average the same.

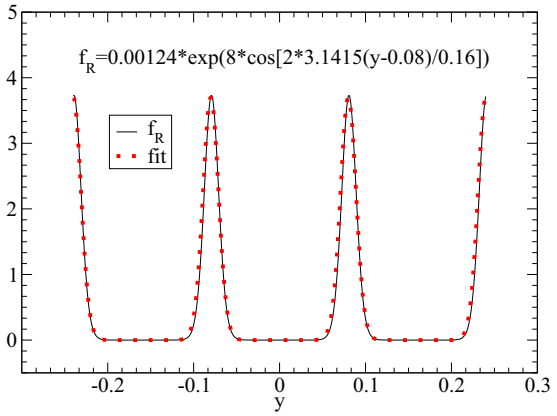

FIG. 13. Fitting of the probe function of the form $\exp(\lambda \cos(2\pi y/d))$ (dots) to the f_R solution (solid line) for $d = 600$, $L = 0.1$, $S_d = 0.16$, and $\alpha = \pi/2$.

instance, in [23,24]. It reads

$$f(y) = N \exp\left(\lambda \cos\left(\frac{2\pi y}{d}\right)\right). \tag{19}$$

We call it the cosine-exponent (CE) function.

Fitting of this function to our results for a chosen set of parameters for a very dense system is given in Fig. 13. Indeed, the function of the type in Eq. (19) seems to be a very satisfactory choice, which requires only three adjustable parameters. We believe that in the case of typical smectic profiles the CE function will work also well, but there exist cases when this function may not be appropriate to use, for instance when the smectic layers are incommensurate or consist of bi- or multilayers or when the molecules do not exhibit head-tail symmetry and the resulting distribution profiles would be not symmetrical. Please also note that the replica method is a general idea and can be used for *any* modulated structures, not only smectics. In the case of liquid crystals it can be also used for description of all modulated nematics, starting from the simple case of cholesterics, through twist bend and splay bend phases, and to other more sophisticated phases that have been recently discovered theoretically [34].

V. SUMMARY

A simple replica method for calculating smectic properties has been presented and examined for studying properties of a two-dimensional needlelike boomerang system. It is based on the observation that the integral equations, whose terms are based on different intervals of the spatial integration, can be, in practice, solved by making replicas of the main box characteristics. It has turned out that the necessary continuity condition required on the distributions at the borders of the central and replica intervals is fulfilled automatically at the end of the convergence process, even though the intermediate or initial steps are discontinuous. This feature of discontinuity at initial stages was probably the reason why the idea with replicas has not been used so far in solving Onsager equations. The iteration process applied to the Onsager self-consistency equations always provides solutions as one or a multiple of

periods with respect to the size of the central integration box S_d. This size can be chosen arbitrarily, yet the minimum of the free energy allows one to find the optimal value of S_d.

Based on the distribution functions, other physical properties, like the above mentioned free energy or order parameters, can be calculated. Distribution functions obtained have been next fitted to the probe CE function used, for instance, in [24]. It turns out that the CE function can be very well fitted to our exact results. There are, however, cases when it is not possible to use the cosine-exponent function and the current algorithm aimed at the exact solutions may be more useful. To such cases belong more complex phases like incommensurate smectic phases, bi- or multilayer smectics, or smectics with asymmetrical profiles of the density peaks. The third case, which, to our knowledge, has not been described yet, is quite plausible and expected to be found, for instance, in polar systems of asymmetrical particles.

To conclude, the above presented approach combined in a complementary way with the CE method has very good perspectives for studying different classes of smectic properties. Not only does it surpass the method of Fourier expansions of interaction terms by allowing for inclusion of all the interaction contribution, but it is also capable of studying incommensurate phases.

In order to extend investigations to a more general description, investigations are currently being carried out to include the whole angle dependence. It is a challenging numerical task to include more variables into the Onsager formalism. The case presented in this paper considers in fact only two orientations of the polar angle. Only the uniaxial smectic phase would require consideration of the whole range of the polar angle, which already extends the time of calculation to several times the computational time needed in the current work. Application of Gaussian quadratures, which are less time consuming, gives hope for the Onsager analysis of the biaxial order.

ACKNOWLEDGMENTS

This work was supported by Grant No. DEC-2013/11/B/ST3/04247 of the National Science Centre in Poland.

[1] P. G. de Gennes and J. Prost, *The Physics of Liquid Crystals* (Oxford University Press, Oxford, UK, 1993).
[2] R. Evans, Adv. Phys. **28**, 143 (1979).
[3] L. Onsager, Ann. N.Y. Acad. Sci. **51**, 627 (1949).
[4] W. Maier and A. Saupe, Z. Naturforsch. A **13**, 564 (1958).
[5] B. Mulder, Phys. Rev. A **39**, 360 (1989).
[6] P. I. C. Teixeira, A. Masters, and B. Mulder, Mol. Cryst. Liq. Cryst. **323**, 167 (1998).
[7] W. L. McMillan, Phys. Rev. A **4**, 1238 (1971).
[8] R. G. Marguta, E. Martín del Río, and E. de Miguel, J. Phys.: Condens. Matter **18**, 10335 (2006).
[9] L. Longa, J. Chem. Phys. **85**, 2974 (1986).
[10] L. V. Mirantseva, Liq. Cryst. **4**, 549 (1989).
[11] J. Chen and T. C. Lubensky, Phys. Rev. A **14**, 1202 (1976).
[12] C. C. Huang and S. Dumrongrattana, Phys. Rev. A **34**, 5020 (1986).
[13] T. Kyu, H.-W. Chiu, and T. Kajiyama, Phys. Rev. E **55**, 7105 (1997).
[14] A. S. Govind and N. V. Madhusudana, Europhys. Lett. **55**, 505 (2001).
[15] M. Osipov and G. Pająk, Phys. Rev. E **85**, 021701 (2012).
[16] K. Trojanowski, G. Pająk, L. Longa, and T. Wydro, Phys. Rev. E **86**, 011704 (2012).
[17] G. Pająk and M. A. Osipov, Phys. Rev. E **88**, 012507 (2013).
[18] A. V. Emelyanenko and A. R. Khokhlov, J. Chem. Phys. **142**, 204905 (2015).
[19] A. Poniewierski and T. J. Sluckin, Mol. Cryst. Liq. Cryst. **212**, 61 (1992).
[20] H. Graf and H. Löwen, J. Phys.: Condens. Matter **11**, 1435 (1999).
[21] E. Velasco, L. Mederos, and T. J. Sluckin, Liq. Cryst. **20**, 399 (1996).
[22] S. Belli, S. Dussi, M. Dijkstra, and R. van Roij, Phys. Rev. E **90**, 020503(R) (2014).
[23] E. Velasco, L. Mederos, and D. E. Sullivan, Phys. Rev. E **62**, 3708 (2000).
[24] Y. Martínez-Ratón and E. Velasco, J. Chem. Phys. **129**, 054907 (2008).
[25] A. Chrzanowska, J. Comput. Phys. **191**, 265 (2003).
[26] E. Velasco and L. Mederos, J. Chem. Phys. **109**, 2361 (1998).
[27] A. Chrzanowska, P. Teixeira, H. Ehrentraut, and D. J. Cleaver, J. Phys.: Condens. Matter **13**, 4715 (2001).
[28] D. J. Cleaver and P. I. C. Teixeira, Chem. Phys. Lett. **338**, 1 (2001).
[29] P. I. C. Teixeira, F. Barmes, C. Anquetil-Deck, and D. J. Cleaver, Phys. Rev. E **79**, 011709 (2009).
[30] P. I. C. Teixeira, A. Chrzanowska, G. D. Wall, and D. J. Cleaver, Mol. Phys. **99**, 889 (2001).
[31] P. Karbowniczek, M. Cieśla, L. Longa, and A. Chrzanowska, Liquid Crystals **44**, 254 (2017).
[32] A. Chrzanowska, Acta Phys. Pol. B **44**, 91 (2013).
[33] A. Chrzanowska, Ferroelectrics **495**, 43 (2016).
[34] L. Longa and G. Pająk, Phys. Rev. E **93**, 040701(R) (2016).